A density functional tight binding model with an extended basis set and three-body repulsion for hydrogen under extreme thermodynamic conditions

Srinivasan, Sriram Goverapet; Goldman, Nir; Tamblyn, Isaac; Hamel, Sebastien; Gaus, Michael

Publisher's version / Version de l'éditeur:
https://doi.org/10.1021/jp5036713
The Journal of Physical Chemistry A, 118, 29, pp. 5520-5528, 2014-06-24

THE JOURNAL OF PHYSICAL CHEMISTRY A

Article

pubs.acs.org/JPCA

A Density Functional Tight Binding Model with an Extended Basis Set and Three-Body Repulsion for Hydrogen under Extreme Thermodynamic Conditions

Sriram Goverapet Srinivasan,[†] Nir Goldman,*[,‡] Isaac Tamblyn,[§] Sebastien Hamel,[‡] and Michael Gaus[∥]

[†]Department of Mechanical and Nuclear Engineering, The Pennsylvania State University, University Park, Pennsylvania 16802, United States

[‡]Physical and Life Sciences Directorate, Lawrence Livermore National Laboratory, Livermore, California 94550, United States

[§]University of Ontario Institute of Technology, Oshawa, Ontario, Canada L1H7K4

[∥]Department of Chemistry, University of Wisconsin-Madison, Madison, Wisconsin 53706, United States

ABSTRACT: We present a new DFTB-p3b density functional tight binding model for hydrogen at extremely high pressures and temperatures, which includes a polarizable basis set (*p*) and a three-body environmentally dependent repulsive potential (*3b*). We find that use of an extended basis set is necessary under dissociated liquid conditions to account for the substantial p-orbital character of the electronic states around the Fermi energy. The repulsive energy is determined through comparison to cold curve pressures computed from density functional theory (DFT) for the hexagonal close-packed solid, as well as pressures from thermally equilibrated DFT-MD simulations of the liquid phase. In particular, we observe improved agreement in our DFTB-p3b model with previous theoretical and experimental results for the shock Hugoniot of hydrogen up to 100 GPa and 25000 K, compared to a standard DFTB model using pairwise interactions and an s-orbital basis set, only. The DFTB-p3b approach discussed here provides a general method to extend the DFTB method for a wide variety of materials over a significantly larger range of thermodynamic conditions than previously possible.

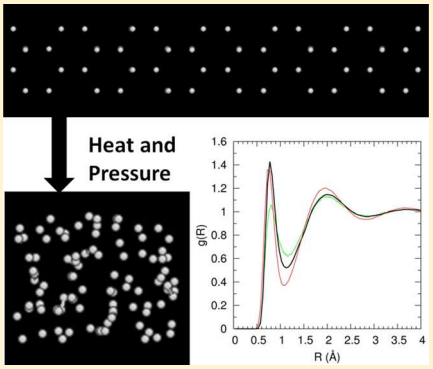

I. INTRODUCTION

Accurate knowledge of the thermophysical properties of hydrogen and its isotopes from ambient conditions to hundreds of GPa and tens of thousands of Kelvin is essential to derive reliable models of the interiors of Jupiter, Saturn, and other giant extra solar planets.[1,2] In addition, isotopes of hydrogen are used as target materials in inertial confinement fusion experiments at the National Ignition Facility (NIF).[3,4] Polymeric materials with high hydrogen content are frequently used in laser-driven dynamic compression experiments in order to drive the compression wave through the samples being studied.[5] Knowledge of the high pressure−temperature behavior of C/H/O/N interactions is necessary to model the behavior of organic energetic materials and in the studies of origins of life through cometary impact,[6−8] where the physical and chemical properties of hydrogen under these conditions plays a significant role in the formation of recoverable chemical products. Shock compression experiments using gas guns,[9,10] explosives,[11,12] magnetically driven flyer plate,[13−15] and lasers[16−19] have been used to obtain optical properties and the pressure−density−temperature Hugoniot relations of hydrogen, and to elucidate the transition of different isotopes from semiconducting to metallic liquid phases at high pressures. (The Hugoniot is the locus of thermodynamic end states achieved by a specific shock velocity and a given set of initial thermodynamic conditions). However, high pressure experiments tend to rely on equation of state (EOS) models for interpretation, which can be inaccurate for a number hydrogen-containing materials across the broad pressure and temperature ranges of many studies.[5,20] Determination of experimental temperatures especially remains an unresolved issue, partially due to large uncertainties in the calibration of pyrometric measurements.[21,22]

Independently, theoretical calculations using density functional theory (DFT)[23−27] based molecular dynamics (MD), path integral Monte Carlo (PIMC),[28] and chemical models[29,30] have provided EOS data and information on the melting curve of hydrogen isotopes. While quantum simulation approaches like DFT have been shown to accurately reproduce the principal Hugoniot and chemical reactivity of condensed hydrogen[31,32] and several hydrocarbons systems,[33,34] the intense computational effort of these methods limits studies to nanometer system sizes and picosecond timescales. In contrast, dynamic compression experiments on hydrogen-containing systems span nanosecond timescales and up to micron length scales.[18,19] DFT-MD simulations can con-

Received: April 14, 2014
Revised: June 23, 2014
Published: June 24, 2014

dx.doi.org/10.1021/jp5036713 | *J. Phys. Chem. A* 2014, 118, 5520−5528

sequently be intractable for these types of studies, where chemical reactivity can span the entire timescale of the experiment. Empirical models, though highly computationally efficient, tend to perform poorly for materials and thermodynamic properties outside of their training set and in general cannot capture the thermal electronic excitations that promote chemical reactivity and soften pressures under hot, dense conditions.[33,34] A previous s-orbital basis set, semiempirical tight-binding parametrization for hydrogen was used for simulations up to 74 GPa.[35,36] However, hydrogen is thought to be highly dissociative under these conditions,[37] and the use of a minimal basis set is insufficient for the resulting metallic state,[38] where ion cores can interact via screened (multicenter) Coulombic repulsion. As such, a computationally efficient and yet accurate quantum chemical method for hydrogen would aid in developing capabilities for direct modeling and interpretation of high pressure−temperature experiments on hydrocarbons, polymers, and other hydrogen-containing materials.

The density functional tight binding (DFTB) method[39,40] is an approximate quantum mechanical approach that can provide orders of magnitude reduction in computational cost while retaining most of the accuracy of the Kohn−Sham DFT. Standard DFTB uses a minimal atom-centered basis set and an approximate Hamiltonian obtained by expanding the Kohn−Sham energy functional to second order in charge fluctuations around a neutral, spherical reference charge density.[39,40] The terms in the resulting energy expression are grouped into the band structure energy (E_{BS}; Hamiltonian energy based on the reference density, n_0), Coulomb energy (E_{coul}; energy from charge fluctuations), and repulsive energy (E_{rep}; ion−ion repulsion, and double counting terms from the Hartree and exchange-correlation interactions). Thus, the total system energy is expressed as $E_{tot} = E_{BS}[n_0] + E_{coul}[\delta n] + E_{rep}(\mathbf{R})$. Here, E_{BS} is obtained using a two-center approximation to the electronic potential, and E_{rep} is usually represented by a short-range, pairwise empirical function.[39,40] While DFTB has been shown to give a reasonable picture of chemical reactivity under moderate pressures and temperatures ($T < 4000$K and $P < 200$ GPa),[41−44] its application to carbon under more extreme conditions (up to 2000 GPa and 30000 K) resulted in overestimation of the metallic liquid equation of state by several hundred GPa and a poor representation of the ensuing structural properties.[38] To rectify these issues, Goldman et al. recently developed a DFTB model (called DFTB-p3b) that included an extended, polarizable basis set (up to d orbitals) for carbon along with a three-body, environmentally dependent repulsive potential.[45] The three-body repulsive energy was necessary in order to account for the greater than two-body forces due to electron delocalization present under molten conditions. The DFTB-p3b model for carbon provides an improved description of the electronic states of metallic liquid, as well as accurate shock Hugoniot curves and radial distribution functions (RDFs).[45]

Along similar lines, in this article, we overcome the limitations of current DFTB parametrizations for hydrogen through the development of a new DFTB-p3b model that includes an extended basis set on the hydrogen atoms (s and p orbitals) and a similar environmentally dependent repulsive potential. Our new hydrogen model yields good agreement with chemical and physical properties for the liquid phase under high pressures and temperatures and provides a more accurate description of the electronic states under dissociation. Furthermore, our DFTB-p3b model is found to yield improved capability to compute the shock Hugoniot over a significantly broader range of pressures and temperatures than possible with previous tight-binding approaches. The DFTB-p3b method provides a straightforward way to develop an extended DFTB approach for MD simulations of hydrogen-containing systems, for which DFT simulations could be intractable and classical empirical potentials (both reactive and nonreactive) could have only a limited range of applicability. In this work, we discuss the details of the computational methods employed in this study along with the details of the environmentally dependent repulsive potential used in the DFTB-p3b model. We then discuss the fitting process and analyze results from MD simulations of hydrogen under static and dynamic compression from both DFTB-p3b and a standard DFTB model, with comparison made to experimental and high-level theoretical data where available.

II. COMPUTATIONAL DETAILS AND METHODS

The functional form for the three-body repulsive energy is identical to that used for carbon.[45] We add an environmental dependence to the standard pairwise formalism based on the electrostatic screening principle[46,47] to account for conditions such as in metallization, where electron delocalization is significant and the two-center approximations inherent in the DFTB approach can be less accurate. In this way, the screening functions are designed to mimic the electrostatic screening effects in solids. E_{rep} is expressed as a sum of pairwise interaction multiplied by a three-body function, viz., $E_{rep} = \sum_i \sum_{j>i} \sum_k V_{ij}(1-S_{ijk})$. V_{ij} is expressed as a ninth-order polynomial.

$$V_{ij} = \begin{cases} \sum_{n=2}^{9} C_n (R_c^{ij} - R_{ij})^n, & R_{ij} < R_c^{ij} \\ 0, & \text{otherwise} \end{cases}$$

The constants labeled C_n correspond to the polynomial coefficients, and R_c^{ij} is the pairwise cutoff radius, beyond which V_{ij} and its derivative are equal to zero. S_{ijk} is the screening factor and is expressed as the product of a sixth-order polynomial and a hyperbolic tangent

$$S_{ijk} = \begin{cases} \left[\sum_{m=0}^{6} b_m \left(R_c^{ijk} - \frac{R_{ik}+R_{jk}}{2}\right)^m\right] & \frac{R_{ik}+R_{jk}}{2} < R_c^{ijk} \\ \quad \tanh\left[a_1 \exp\left(-a_2 \left(\frac{R_{ik}+R_{jk}}{R_{ij}}\right)^{a_3}\right)\right], & \\ 0, & \text{otherwise} \end{cases}$$

The constants labeled b_m are the polynomial coefficients while a_1, a_2, and a_3 are additional coefficients to be fit. R_c^{ijk} is the three-body interaction cutoff radius. Both the pairwise and three-body cutoff radii ensure smooth behavior around R_c^{ij} and R_c^{ijk} and that the functions will be equal to zero beyond. The coefficients b_m were constrained during fitting to yield values of S_{ijk} between 0 and 1. As a result, the repulsive potential between atoms i and j is completely screened and equal to zero when an atom k within radius R_c^{ijk} exists at the midpoint of the line joining atomic centers i and j, while the function recovers its pairwise form when the third atom k exists beyond R_c^{ijk} (Figure 1).

Similar to our previous work,[38,45] all DFTB type simulations were driven by the LAMMPS molecular simulation suite,[48,49]

dx.doi.org/10.1021/jp5036713 | J. Phys. Chem. A 2014, 118, 5520−5528

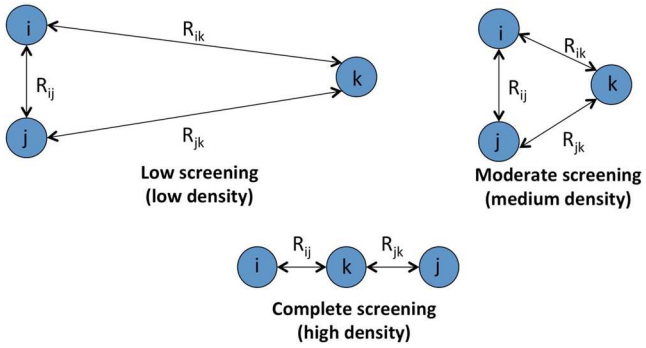

Figure 1. Illustration of the screening principle used in development of our three-body repulsive energy.[45] At low density $[(R_{ik} + R_{jk})/2 > R_c^{ijk}]$, screening from atom k is relatively small, and the repulsive energy between atoms i and j is approximately pairwise. At high density, atom k can completely screen the repulsive energy interaction between atoms i and j.

with the DFTB+ code[50] used to calculate the total energy terms excluding E_{rep} (i.e., E_{BS} and E_{Coul}) and LAMMPS used to compute the repulsive energy terms as well as drive the MD calculations. For the sake of comparison with a standard DFTB model using a minimal basis set implementation (i.e., s orbitals, only) and a pairwise repulsive energy function, we used the mio-0−1 parameter set for hydrogen,[39] available for download from http://www.dftb.org. Both sets of DFTB type calculations (DFTB-mio and DFTB-p3b) were performed with self-consistent charges (SCC).[39] All of our calculations were initiated in an ordered hcp lattice, which readily melted into a liquid phase upon application of the high temperatures of our MD studies. All geometry optimizations with DFTB were performed with force convergence criteria of 10^{-6} kcal/mol Å and SCC convergence criteria of 10^{-6} or smaller. DFT simulations were performed using the VASP[51−54] plane wave basis set based DFT code, with projector augmented wave (PAW) pseudopotentials,[55,56] the Perdew−Burke−Ernzerhof generalized gradient approximation functional,[57,58] and a 900 eV plane wave cutoff. For our VASP calculations, the wave function convergence criteria was set to10^{-4} eV and the force convergence criteria was set to 10^{-3} eV/Å.

The Mermin functional[59] was used to compute fractional electron occupations for all systems and simulation methods. For our cold curve calculations the electronic temperature was fixed at a value of 0.03 eV, whereas for all of our MD simulations it was set to the ionic temperature of the system. All cold curve calculations were computed using a system consisting of four hydrogen molecules (8 atoms total) arranged in a hexagonal close packed (HCP) lattice. The Brillouin zone was sampled using a 10 × 10 × 10 k point mesh using the Monkhorst−Pack[60] sampling scheme, though results at high density were found to be converged with an 8 × 8 × 8 mesh. Our MD simulations with DFTB-SCC were all performed using the extended Lagrangian Born−Oppenheimer molecular dynamics (XL-BOMD) technique to propagate the electronic degrees of freedom.[61−65] This allowed us to reduce the maximum number of SCC steps to 5 per MD time step, though in general, simulations with as few as three SCC steps were found to allow for stable conserved quantities in our simulations.

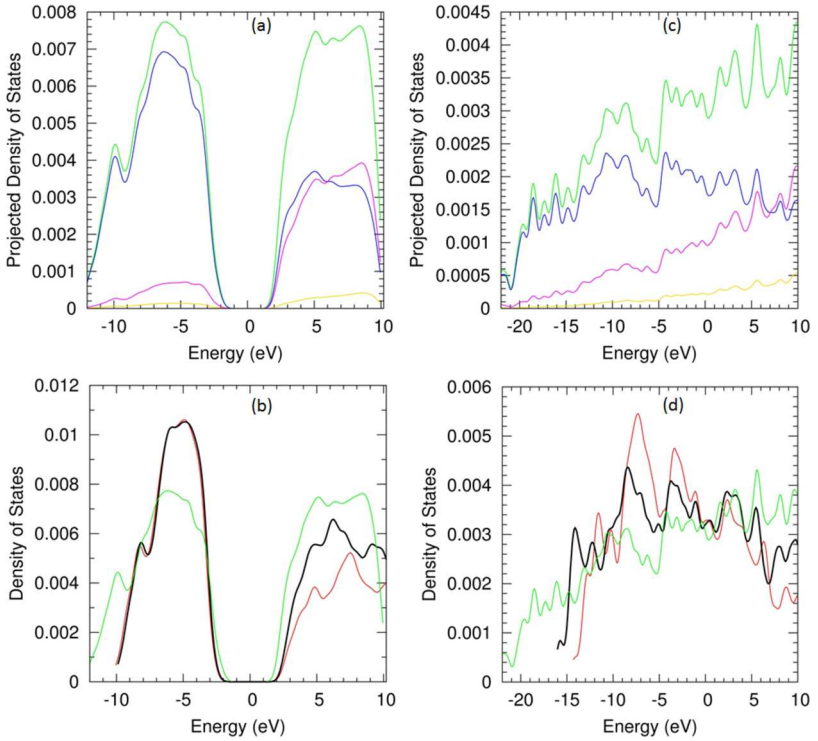

Figure 2. Projected density of states from DFT and the total electronic density of states from DFT, DFTB-mio, and DFTB-p3b. All plots are aligned by setting the Fermi energy equal to zero. The curves in (a and c) show the projected density of states from DFT for a liquid snapshot at 0.3 g/cm^3 at 2000 K and 0.7 g/cm^3 at 7000 K, respectively. The curves in (b and d) show the total density of states computed from DFT, DFTB-mio, and DFTB-p3b for the same configurations. The green line in all plots corresponds to the total DOS from DFT. Blue, pink, and yellow lines in (a and c) correspond to s, p, and d orbital PDOS results, respectively. Black and red lines in (b and d) correspond to the total DOS from DFTB-p3b and DFTB-mio, respectively.

dx.doi.org/10.1021/jp5036713 | J. Phys. Chem. A 2014, 118, 5520−5528

III. RESULTS AND DISCUSSION

In order to assess the importance of including an expanded basis set in our calculations, we have computed the projected electronic density of states (PDOS) from DFT and the total electronic density of states (DOS) from DFTB-p3b and DFTB-mio using thermally equilibrated configurations from DFT-MD simulations. We have analyzed results from DFT-MD simulations for a molecular liquid (0.3 g/cm^3, 2000 K) as well as one that is highly dissociated and metallic (0.7 g/cm^3, 7000 K). The total DOS from our tight-binding calculations are independent of E_{rep}, allowing for a direct comparison to density of states results from DFT without any empirical function fitting. PDOS results from DFT indicate that for the molecular liquid state, the occupied states are largely well represented by s-orbitals, with the p-orbitals making more significant contributions to the unoccupied states, and d orbitals contributing only small amounts over the entire computed energy spectrum (Figure 2a). Correspondingly, for the molecular liquid both DFTB-p3b and DFTB-mio are able to replicate the general morphology of the DOS curve from DFT, though DFTB-mio underestimates the density of unoccupied states to a larger degree and both DFTB-mio and DFTB-p3b yield slightly larger values for the system band gap (Figure 2b).

In contrast, p-orbital interactions become significant for the occupied states under dissociative conditions (Figure 2c), where the system is metallic and thermal electronic excitations that affect the heat capacity and system pressure readily occur. For example, the p-orbital character of electronic states near the Fermi energy increases from approximately 14% for the molecular liquid state to approximately 30% under metallic conditions. The d-contributions to the electronic states for the dissociative state increase monotonically with increasing energy, though they are not significant until relatively high energy (e.g., greater than 10 eV above the Fermi energy). We observe that DFTB-p3b yields an overall improved description of DOS for the dissociative state relative to DFTB-mio, in particular for both the occupied and unoccupied states within a few eV of the Fermi energy (Figure 2d). DFTB-mio yields a DOS curve somewhat similar to the s-orbital PDOS results from DFT at these conditions, which decreases monotonically at the Fermi energy and beyond.

Optimization of the three-body repulsive energy was performed through simulated annealing[66,67] utilizing a data set consisting of pressures from a DFT-computed cold curve for hydrogen from 0.3 g/cm^3 to 0.7 g/cm^3, along with pressures from configurations taken from DFT-MD simulations of liquid hydrogen spanning densities of 0.3 g/cm^3 to 0.7 g/cm^3 and temperatures of 2000 K to 7000 K. Higher pressures and temperatures are known to have significant three-body contributions to the total energy of the system, particularly under dissociative/metallic conditions, which promote increased coordination of the hydrogen atoms.[45] Our repulsive energy parameters are given in Table 1. The resulting repulsive energy was in general able to match the liquid pressure points in our data set all within a few GPa. Cold curve (zero Kelvin compression) data from DFTB-p3b represents a substantial improvement over DFTB-mio (Figure 3), though pressures are between 5 and 10% lower than those from our DFT calculations at 0.6 and 0.7 g/cm^3, as well as results from an experimentally determined EOS based on isothermal compression of solid hydrogen at 300 K.[70] However, our results compare closely at all densities with those from an ab initio multiphase equation of state.[68] In addition, the PBE exchange-correlation functional is known to overestimate system pressures at higher densities.[69]

Table 1. Values of the Parameters in the Environment Dependent Repulsive Potential in Atomic Units

parameters for the pairwise component		parameters for the three-body screening component	
parameter	value (au)	parameter	value (au)
C_2	0.020592	b_2	8.410065
C_3	−0.042896	b_3	−14.598 81
C_4	0.003471	b_4	8.613503
C_5	0.160235	b_5	−0.997082
C_6	−0.246144	b_6	−0.423197
C_7	0.155087	a_1	24.295529
C_8	−0.045205	a_2	5.071158
C_9	0.005144	a_3	4.166714
R_c^{ij}	3.212534	R_c^{ijk}	2.644956

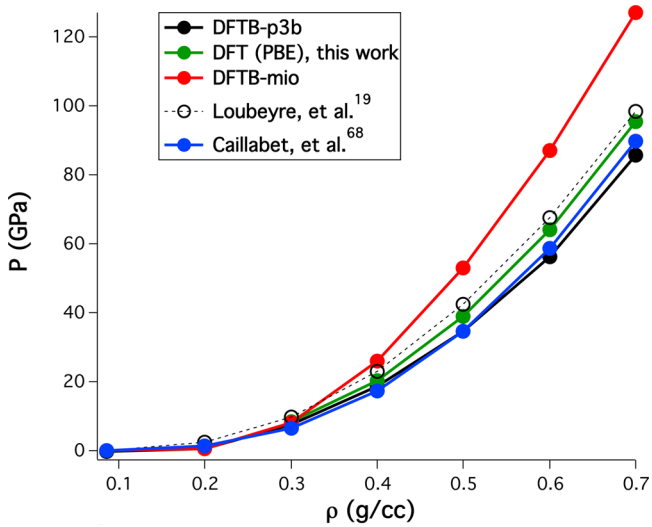

Figure 3. Zero Kelvin compression data comparing DFTB-p3b to other theoretical and experimental results. DFTB-p3b represents a significant improvement over DFTB-mio and compares well to the ab initio EOS from Caillabet et al.[68] However, DFTB-p3b yields an equation of state that is 5−10% softer than the experimental results from Loubeyre et al.[70] and our own DFT results.

We have tested our new three-body repulsive energy by conducting constant volume and temperature simulations (NVT-MD) with DFTB-p3b and DFTB-mio on a system consisting of 108 hydrogen molecules (216 atoms) initially arranged in an HCP lattice. Here, we have simulated densities of 0.3 g/cm^3 to 0.7 g/cm^3 in steps of 0.1 g/cm^3 and temperatures of 2000 to 7000 K in steps of 1000 K. Results were compared to a previously computed data set of DFT-MD simulations on a system consisting of 125 Hydrogen molecules at identical conditions. All MD simulations were performed for a duration of 20 ps using a time step of 0.2 fs, with the Nose−Hoover thermostat[71,72] and Γ-point sampling of the Brillouin zone. Use of a 4 × 4 × 4 k-point mesh for DFT calculations under metallic conditions resulted in deviations in the total energy and pressure of approximately 1% or less.

Our results indicate that DFTB-mio yields excessively high pressures at all simulated conditions, ranging from 13.9% at 0.3 g/cm^3 and 2000 K to a peak deviation of 45.8% at 0.6 g/cm^3 and 4000 K (Table 2). This is part due to the fact that the

dx.doi.org/10.1021/jp5036713 | J. Phys. Chem. A 2014, 118, 5520−5528

Table 2. Comparison of the Pressures from NVT-MD Simulations Using DFT, DFTB-mio, and DFTB-p3b

	2000 K			4000 K			7000 K		
	DFT (GPa)	DFTB-mio (GPa)	DFTB-p3b (GPa)	DFT (GPa)	DFTB-mio (GPa)	DFTB-p3b (GPa)	DFT (GPa)	DFTB-mio (GPa)	DFTB-p3b (GPa)
0.3 g/cm^3	16.05	18.28 (±0.83)	15.29 (±0.91)	20.34	23.50 (±1.24)	19.83 (±1.26)	23.47	30.23 (±1.58)	26.62 (±1.55)
0.4 g/cm^3	31.04	38.81 (±1.08)	29.19 (±1.21)	33.63	45.52 (±1.54)	35.64 (±1.57)	40.42	55.74 (±2.03)	46.14 (±1.97)
0.5 g/cm^3	51.93	67.41 (±1.39)	47.84 (±1.41)	52.33	75.70 (±1.87)	56.51 (±1.91)	64.51	89.92 (±2.39)	71.34 (±2.53)
0.6 g/cm^3	78.04	104.08 (±1.52)	72.24 (±1.64)	77.92	113.61 (±2.13)	83.44 (±2.34)	96.56	131.54 (±2.88)	102.81 (±3.06)
0.7 g/cm^3	104.20	146.63 (±1.58)	103.84 (±2.0)	112.11	157.69 (±2.39)	117.67 (±2.79)	136.21	179.56 (±3.30)	141.93 (±3.68)

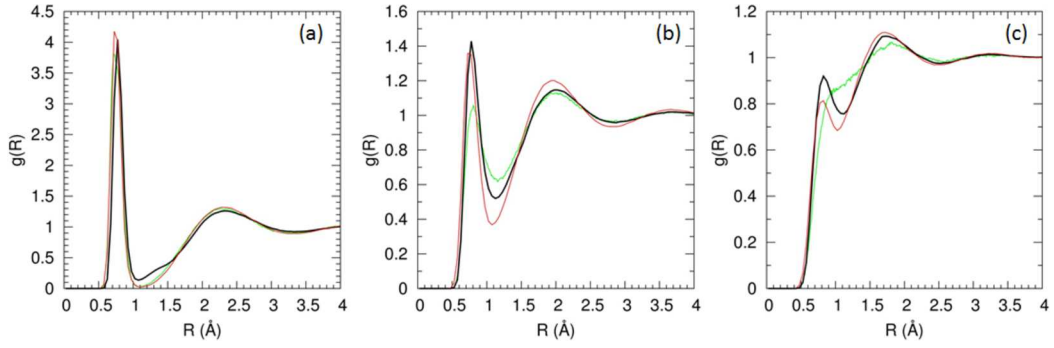

Figure 4. Comparison of the RDFs from DFT (green), DFTB-mio (red), and DFTB-p3b (black). (a–c) show the RDFs computed from an NVT-MD simulation at 0.3 g/cm^3 and 2000 K, 0.5 g/cm^3 and 4000 K, and 0.7 g/cm^3 and 7000 K respectively.

coordination number for the first solvation shell increases beyond the expected value of one at high density (e.g., a value of 1.5 at 0.7 g/cm^3, 7000 K) due to the dissociation of hydrogen molecules, which can yield unphysically high stresses in calculations limited to s-orbital interactions, exclusively. These high stress effects were likely not included in the parametrization of the DFTB-mio repulsive energy. In contrast, use of p orbitals in DFTB-p3b allows for configurations with more than one nearest neighbor to form with lower stresses, all of which have been incorporated into our fit for the DFTB-p3b system pressures. Consequently, the DFTB-p3b model yields significantly more accurate equation of state properties for condensed phase hydrogen and predicts pressures that are generally within 5 GPa of those from DFT under these conditions.

In general, we observe good agreement between the RDFs from DFTB-p3b and DFT, particularly for conditions of the molecular liquid, where there is little to no H_2 dissociation from these models (Figure 4). The RDF from both DFTB-mio and DFTB-p3b are in good agreement with DFT at 0.3 g/cm^3 and 2000 K. At 0.5 g/cm^3 and 4000 K, the RDF from both DFTB-mio and DFTB-p3b yielded a similarly overstructured first peak, but DFTB-p3b gives an improved description for the first minimum and the subsequent structure in comparison to DFT. At 0.7 g/cm^3 and 7000 K, both DFTB-mio and DFTB-p3b give a distinct peak at around 0.75 Å that is absent in DFT. This first peak is indicative of a smaller percentage of molecular dissociation predicted by these methods, where the hydrogen molecules in our DFT-MD results are almost entirely dissociated under these conditions. However, the PBE functional is known to greatly overestimate dissociation and metallization in the liquid phase of hydrogen[69,73] and results from DFTB-p3b could be more in line with more accurate but extremely computationally intensive approaches (which are beyond the scope of this study).

We have examined the properties due to dynamic compression from DFTB-p3b by computing the high pressure–temperature Hugoniot relations for solid hydrogen shock compressed to the liquid phase. Quasi-isentropic compressions access high pressure, low temperature states related to the interior of giant planets and to experiments on NIF and could provide an avenue for future work.[74] Shock compression simulations were carried out on a system consisting of 48 hydrogen molecules (96 atoms) arranged in an HCP lattice corresponding to an initial density of 0.08 g/cm^3. Simulations with both DFTB models were carried out using the multiscale shock simulation technique (MSST),[75−77] including modifications to allow for the coupling of electronic and ionic temperature in the simulation.[78] MSST simulations have been shown to accurately reproduce the Hugoniot of a number of different reactive systems,[79,80] including the sequence of thermodynamic states throughout the reaction zone upon shock compression of energetic mixtures.[77] The system was equilibrated at 5 K using Nose–Hoover thermostat for a duration of 20 ps before subjecting it to shock compression. All shock compression simulations were run for durations of 50 ps using a time step of 0.2 fs, with Γ-point sampling only. Similar to previous work,[45] use of scaling factors of 10^{-4} resulted in drifts in the Hugoniot energy condition and Rayleigh line that were less than 3% without affecting the total forces in our simulations. We have simulated shock speeds from 10 to 25 km/s in steps of 1 km/s and shock velocities of 30, 35, and 40 km/s using the DFTB-p3b method while shock speeds up to 25 km/s only were simulated using the DFTB-mio method. Beyond a shock velocity of 25 km/s, our DFTB-mio simulations resulted in excessively large drifts off the Hugoniot

dx.doi.org/10.1021/jp5036713 | J. Phys. Chem. A 2014, 118, 5520−5528

(≫ 5%). This is likely due to the minimal s-orbital basis set, which yields too strong repulsive stresses under these dissociative conditions and resulted in unphysical interatomic forces that were difficult to resolve.

For the pressure versus density Hugoniot (Figure 5), DFTB-p3b is in good agreement with the experimental data of Nellis et al.[9] and Sano et al.[18] at lower pressures (< 30 GPa) and Loubeyre et al.[19] and Knudson et al.[14] at higher pressures. DFTB-p3b also agrees with the Path Integral Monte Carlo data of Militzer et al.[28] and is in reasonable agreement with the DFT data of Desjarlais[24] and Holst et al.[27] DFTB-p3b, however, does not show a maximum in the compression ratio for hydrogen seen in results of Sano et al.[18] and Loubeyre et al.[19] between pressures of 40 and 60 GPa. In contrast, DFTB-mio generally yields a stiffer equation of state than DFTB-p3b, though its pressure predictions at lower conditions are still within experimental error bars. However, 40 GPa was approximately the maximum Hugoniot pressure achievable with these simulations, whereas DFTB-p3b is able to yield accurate equation of state results to 100 GPa and beyond.

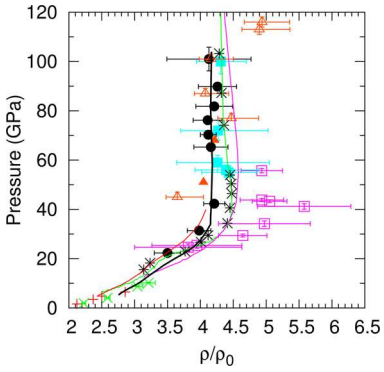

Figure 5. Comparison of the principal Hugoniot from DFTB-p3b (black line) and DFTB-mio (red line) with experimental and theoretical data reported in literature. Experiment (H_2 data): Dick et al.[11] (+), Nellis et al.[9] (×), Sano et al.[18] (□), Loubeyre et al.[19] (■, P_0 = 0.3 GPa). Experiment (D_2 data): Knudson et al.[14] (●), Hicks et al.[17] (△). Theory (H_2 data): Holst et al.[27] (green line). Theory (D_2 data): Desjarlais et al.[24] (black stars), Militzer et al.[28] (orange-filled ▲), Lenosky et al.[23] (pink line).

The temperature versus density Hugoniot from DFTB-p3b is in good agreement with one set of experimental results[15] (Figure 6), though it is somewhat lower than shock compression studies on a precompressed sample at temperatures of 12000 K and greater.[19] H_2 molecular bonds can persist at more extreme conditions than predicted by calculations with the PBE functional.[69] Neglect of quantum nuclear vibrational effects in covalently bonded systems is known to cause Hugoniot temperatures to be underestimated in covalently bonded systems.[81,82] The temperatures predicted by DFTB-mio are in good agreement with DFTB-p3b at pressures less than 20 GPa, though the model yields lower values at higher pressures, consistent with harder Hugoniot curves overall. We have also computed the shock velocity (U_s) versus particle velocity (U_p) Hugoniot (Figure 7) from DFTB-p3b and DFTB-mio using the relation $U_p = U_s(1 - \rho_0/\rho)$, where ρ_0 corresponds to the density of the preshock, initial state. Our results from DFTB-p3b are in good agreement with other data reported in the literature for shock velocities up to 30 km/s, beyond which there is a small deviation in the curve compared to the experiments.

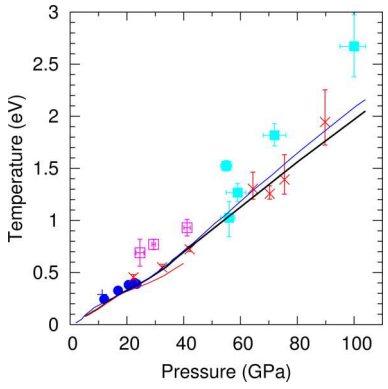

Figure 6. Comparison of the temperature along the principal Hugoniot from DFTB-p3b (black line) and DFTB-mio (red line) with data reported in the literature. H_2 data: Holmes et al.[10] (+), Sano et al.[18] (□), Loubeyre et al.[19] (■, P_0 = 0.3 GPa). D_2 data: Holmes et al.[10] (●), Bailey et al.[15] (×).

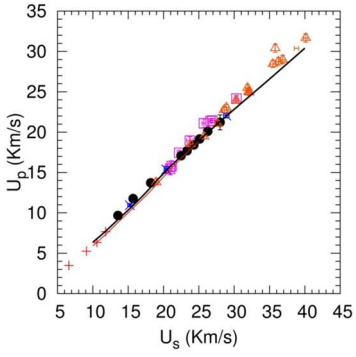

Figure 7. Comparison of the U_s vs U_p relationship from DFTB-p3b (black line) and DFTB-mio (red line) with data reported in the literature. H_2 data: Dick et al.[11] (+), Sano et al.[18] (□). D_2 data: Knudson et al.[14] (●), Boriskov et al.[12] (×), Hicks et al.[17] (△).

IV. CONCLUSIONS

We have created a new density functional tight binding model for hydrogen (DFTB-p3b) that uses an extended basis set (s and p orbitals) and an environmentally dependent repulsive potential for condensed phases under extreme pressures and temperatures. The expanded basis set improves upon previous DFTB parametrizations by providing a more accurate description of electronic states under these conditions, particularly for state points where molecular hydrogen is largely dissociated. Our three-body repulsive energy yields pressures and radial distribution functions that are substantially improved over previous DFTB implementations and are in good agreement with DFT computed data for conditions ranging from 0.3 g/cm^3 and 2000 K to 0.7 g/cm^3 and 7000 K. Furthermore, the shock Hugoniot data computed using DFTB-p3b generally are in good agreement with other experimental and theoretical data reported in literature, yielding accurate results that were tested up to 100 GPa and 25000 K. Our DFTB-p3b approach provides a general, straightforward way to extend the DFTB method to a wide variety of materials over a broad range of conditions, including geological and planetary materials such as hydrocarbons, silicon, and SiO_2. The computational efficiency inherent in our models could allow

dx.doi.org/10.1021/jp5036713 | J. Phys. Chem. A 2014, 118, 5520−5528

for simulations of hydrogen-containing materials that approach the timescales of dynamic compression experiments, where physical and chemical properties can be difficult to interrogate directly and there is generally a significant reliance on simulations for interpretation and validation of results.

AUTHOR INFORMATION

Corresponding Author

*E-mail: goldman14@llnl.gov.

Notes

The authors declare no competing financial interest.

ACKNOWLEDGMENTS

This work was performed under the auspices of the U.S. Department of Energy by Lawrence Livermore National Laboratory under Contract DE-AC52-07NA27344 and was funded by Laboratory Directed Research and Development Grant 12-ERD-052 with N.G. as principle investigator. Computations were performed at LLNL using the Aztec and RZCereal massively parallel computers.

REFERENCES

(1) Guillot, T. Interiors of Giant Planets Inside and Outside the Solar System. *Science* **1999**, *286*, 72−77.
(2) Guillot, T. A Comparison of the Interiors of Jupiter and Saturn. *Planet. Space Sci.* **1999**, *47*, 1183−1200.
(3) Lindl, J. D.; Amendt, P.; Berger, R. L.; Glendinning, S. G.; Glenzer, S. H.; Haan, S. W.; Kauffman, R. L.; Landen, O. L.; Suter, L. J. The Physics Basis for Ignition Using Indirect-Drive Targets on the National Ignition Facility. *Phys. Plasmas* **2004**, *11*, 339−491.
(4) Edwards, M. J.; Patel, P. K.; Lindl, J. D.; Atherton, L. J.; Glenzer, S. H.; Haan, S. W.; Kilkenny, J. D.; Landen, O. L.; Moses, E. I.; Nikroo, A.; et al. Progress Towards Ignition on the National Ignition Facility. *Phys. Plasmas* **2013**, *20*, 070501.
(5) Barrios, M. A.; Hicks, D. G.; Boehly, T. R.; Fratanduono, D. E.; Eggert, J. H.; Celliers, P. M.; Collins, G. W.; Meyerhofer, D. D. High-Precision Measurements of the Equation of State of Hydrocarbons at 1−10 Mbar Using Laser-Driven Shock Waves. *Phys. Plasmas* **2010**, *17*, 056307.
(6) Goldman, N.; Reed, E. J.; Fried, L. E.; William Kuo, I. F.; Maiti, A. Synthesis of Glycine-Containing Complexes in Impacts of Comets on Early Earth. *Nat. Chem.* **2010**, *2*, 949−954.
(7) Martins, Z.; Price, M. C.; Goldman, N.; Sephton, M. A.; Burchell, M. J. Shock Synthesis of Amino Acids from Impacting Cometary and Icy Planet Surface Analogues. *Nat. Geosci.* **2013**, *6*, 1045−1049.
(8) Goldman, N.; Tamblyn, I. Prebiotic Chemistry within a Simple Impacting Icy Mixture. *J. Phys. Chem. A* **2013**, *117*, 5124−5131.
(9) Nellis, W. J.; Mitchell, A. C.; van Thiel, M.; Devine, G. J.; Trainor, R. J.; Brown, N. Equation-of-State Data for Molecular Hydrogen and Deuterium at Shock Pressures in the Range 2−76 GPa (20−760 Kbar). *J. Chem. Phys.* **1983**, *79*, 1480−1486.
(10) Holmes, N. C.; Ross, M.; Nellis, W. J. Temperature Measurements and Dissociation of Shock-Compressed Liquid Deuterium and Hydrogen. *Phys. Rev. B* **1995**, *52*, 15835−15845.
(11) Dick, R. D.; Kerley, G. I. Shock Compression Data for Liquids. Ii. Condensed Hydrogen and Deuterium. *J. Chem. Phys.* **1980**, *73*, 5264−5271.
(12) Boriskov, G. V.; Bykov, A. I.; Il'kaev, R. I.; Selemir, V. D.; Simakov, G. V.; Trunin, R. F.; Urlin, V. D.; Shuikin, A. N.; Nellis, W. J. Shock Compression of Liquid Deuterium up to 109 GPa. *Phys. Rev. B* **2005**, *71*, 092104.
(13) Knudson, M. D.; Hanson, D. L.; Bailey, J. E.; Hall, C. A.; Asay, J. R.; Anderson, W. W. Equation of State Measurements in Liquid Deuterium to 70 GPa. *Phys. Rev. Lett.* **2001**, *87*, 225501.
(14) Knudson, M. D.; Hanson, D. L.; Bailey, J. E.; Hall, C. A.; Asay, J. R.; Deeney, C. Principal Hugoniot, Reverberating Wave, and Mechanical Reshock Measurements of Liquid Deuterium to 400 GPa Using Plate Impact Techniques. *Phys. Rev. B* **2004**, *69*, 144209.
(15) Bailey, J. E.; Knudson, M. D.; Carlson, A. L.; Dunham, G. S.; Desjarlais, M. P.; Hanson, D. L.; Asay, J. R. Time-Resolved Optical Spectroscopy Measurements of Shocked Liquid Deuterium. *Phys. Rev. B* **2008**, *78*, 144107.
(16) Collins, G. W.; Da Silva, L. B.; Celliers, P.; Gold, D. M.; Foord, M. E.; Wallace, R. J.; Ng, A.; Weber, S. V.; Budil, K. S.; Cauble, R. Measurements of the Equation of State of Deuterium at the Fluid Insulator-Metal Transition. *Science* **1998**, *281*, 1178−1181.
(17) Hicks, D. G.; Boehly, T. R.; Celliers, P. M.; Eggert, J. H.; Moon, S. J.; Meyerhofer, D. D.; Collins, G. W. Laser-Driven Single Shock Compression of Fluid Deuterium from 45 to 220 GPa. *Phys. Rev. B* **2009**, *79*, 014112.
(18) Sano, T.; Ozaki, N.; Sakaiya, T.; Shigemori, K.; Ikoma, M.; Kimura, T.; Miyanishi, K.; Endo, T.; Shiroshita, A.; Takahashi, H.; et al. Laser-Shock Compression and Hugoniot Measurements of Liquid Hydrogen to 55 GPa. *Phys. Rev. B* **2011**, *83*, 054117.
(19) Loubeyre, P.; Brygoo, S.; Eggert, J.; Celliers, P. M.; Spaulding, D. K.; Rygg, J. R.; Boehly, T. R.; Collins, G. W.; Jeanloz, R. Extended Data Set for the Equation of State of Warm Dense Hydrogen Isotopes. *Phys. Rev. B* **2012**, *86*, 144115.
(20) Lyzenga, G. A.; Ahrens, T. J.; Nellis, W. J.; Mitchell, A. C. The Temperature of Shock-Compressed Water. *J. Chem. Phys.* **1982**, *76*, 6282−6286.
(21) Lee, K. K. M.; Benedetti, L. R.; Jeanloz, R.; Celliers, P. M.; Eggert, J. H.; Hicks, D. G.; Moon, S. J.; Mackinnon, A.; Da Silva, L. B.; Bradley, D. K.; et al. Laser-Driven Shock Experiments on Precompressed Water: Implications for "Icy" Giant Planets. *J. Chem. Phys.* **2006**, *125*, 014701.
(22) Eggert, J. H.; Hicks, D. G.; Celliers, P. M.; Bradley, D. K.; McWilliams, R. S.; Jeanloz, R.; Miller, J. E.; Boehly, T. R.; Collins, G. W. Melting Temperature of Diamond at Ultrahigh Pressure. *Nat. Phys.* **2010**, *6*, 40−43.
(23) Lenosky, T. J.; Bickham, S. R.; Kress, J. D.; Collins, L. A. Density-Functional Calculation of the Hugoniot of Shocked Liquid Deuterium. *Phys. Rev. B* **2000**, *61*, 1−4.
(24) Desjarlais, M. P. Density-Functional Calculations of the Liquid Deuterium Hugoniot, Reshock, and Reverberation Timing. *Phys. Rev. B* **2003**, *68*, 064204.
(25) Bonev, S. A.; Militzer, B.; Galli, G. Ab Initio Simulations of Dense Liquid Deuterium: Comparison with Gas-Gun Shock-Wave Experiments. *Phys. Rev. B* **2004**, *69*, 014101.
(26) Bonev, S. A.; Schwegler, E.; Ogitsu, T.; Galli, G. A Quantum Fluid of Metallic Hydrogen Suggested by First-Principles Calculations. *Nature* **2004**, *431*, 669−672.
(27) Holst, B.; Redmer, R.; Desjarlais, M. P. Thermophysical Properties of Warm Dense Hydrogen Using Quantum Molecular Dynamics Simulations. *Phys. Rev. B* **2008**, *77*, 184201.
(28) Militzer, B.; Ceperley, D. M. Path Integral Monte Carlo Calculation of the Deuterium Hugoniot. *Phys. Rev. Lett.* **2000**, *85*, 1890−1893.
(29) Ross, M. Linear-Mixing Model for Shock-Compressed Liquid Deuterium. *Phys. Rev. B* **1998**, *58*, 669−677.
(30) Juranek, H.; Redmer, R. Self-Consistent Fluid Variational Theory for Pressure Dissociation in Dense Hydrogen. *J. Chem. Phys.* **2000**, *112*, 3780−3786.
(31) Galli, G.; Hood, R. Q.; Hazi, A. U.; Gygi, F. *Ab Initio* Simulations of Compressed Liquid Deuterium. *Phys. Rev. B* **2000**, *61*, 909−912.
(32) Gygi, F.; Galli, G. Electronic Excitations and the Compressibility of Deuterium. *Phys. Rev. B* **2002**, *65*, 220102.
(33) Mattsson, T. R.; Lane, J. M. D.; Cochrane, K. R.; Desjarlais, M. P.; Thompson, A. P.; Pierce, F.; Grest, G. S. First-Principles and Classical Molecular Dynamics Simulation of Shocked Polymers. *Phys. Rev. B* **2010**, *81*, 054103.
(34) Root, S.; Haill, T. A.; Lane, J. M. D.; Thompson, A. P.; Grest, G. S.; Schroen, D. G.; Mattsson, T. R. Shock Compression of Hydrocarbon Foam to 200 GPa: Experiments, Atomistic Simulations,

and Mesoscale Hydrodynamic Modeling. *J. Appl. Phys.* **2013**, *114*, 103502.
(35) Lenosky, T. J.; Kress, J. D.; Collins, L. A.; Kwon, I. Molecular-Dynamics Modeling of Shock-Compressed Liquid Hydrogen. *Phys. Rev. B* **1997**, *55*, R11907−R11910.
(36) Lenosky, T. J.; Kress, J. D.; Collins, L. A. Molecular-Dynamics Modeling of the Hugoniot of Shocked Liquid Deuterium. *Phys. Rev. B* **1997**, *56*, 5164−5169.
(37) Tamblyn, I.; Bonev, S. A. A Note on the Metallization of Compressed Liquid Hydrogen. *J. Chem. Phys.* **2010**, *132*, 134503.
(38) Goldman, N.; Fried, L. E. Extending the Density Functional Tight Binding Method to Carbon under Extreme Conditions. *J. Phys. Chem. C* **2012**, *116*, 2198−2204.
(39) Elstner, M.; Porezag, D.; Jungnickel, G.; Elsner, J.; Haugk, M.; Frauenheim, T.; Suhai, S.; Seifert, G. Self-Consistent-Charge Density-Functional Tight-Binding Method for Simulations of Complex Materials Properties. *Phys. Rev. B* **1998**, *58*, 7260−7268.
(40) Porezag, D.; Frauenheim, T.; Köhler, T.; Seifert, G.; Kaschner, R. Construction of Tight-Binding-Like Potentials on the Basis of Density-Functional Theory: Application to Carbon. *Phys. Rev. B* **1995**, *51*, 12947−12957.
(41) Reed, E. J.; Riad Manaa, M.; Fried, L. E.; Glaesemann, K. R.; Joannopoulos, J. D. A Transient Semimetallic Layer in Detonating Nitromethane. *Nat. Phys.* **2008**, *4*, 72−76.
(42) Manaa, M. R.; Fried, L. E.; Melius, C. F.; Elstner, M.; Frauenheim, T. Decomposition of HMX at Extreme Conditions: A Molecular Dynamics Simulation. *J. Phys. Chem. A* **2002**, *106*, 9024−9029.
(43) Margetis, D.; Kaxiras, E.; Elstner, M.; Frauenheim, T.; Manaa, M. R. Electronic Structure of Solid Nitromethane: Effects of High Pressure and Molecular Vacancies. *J. Chem. Phys.* **2002**, *117*, 788−799.
(44) Manaa, M. R.; Reed, E. J.; Fried, L. E.; Goldman, N. Nitrogen-Rich Heterocycles as Reactivity Retardants in Shocked Insensitive Explosives. *J. Am. Chem. Soc.* **2009**, *131*, 5483−5487.
(45) Goldman, N.; Goverapet Srinivasan, S.; Hamel, S.; Fried, L. E.; Gaus, M.; Elstner, M. Determination of a Density Functional Tight Binding Model with an Extended Basis Set and Three-Body Repulsion for Carbon under Extreme Pressures and Temperatures. *J. Phys. Chem. C* **2013**, *117*, 7885−7894.
(46) Tang, M. S.; Wang, C. Z.; Chan, C. T.; Ho, K. M. Environment-Dependent Tight-Binding Potential Model. *Phys. Rev. B* **1996**, *53*, 979−982.
(47) Haas, H.; Wang, C. Z.; Fähnle, M.; Elsässer, C.; Ho, K. M. Environment-Dependent Tight-Binding Model for Molybdenum. *Phys. Rev. B* **1998**, *57*, 1461−1470.
(48) Plimpton, S. Fast Parallel Algorithms for Short-Range Molecular Dynamics. *J. Comput. Phys.* **1995**, *117*, 1−19.
(49) LAMMPS Molecular Dynamics Simulator. http://lammps.sandia.gov.
(50) Aradi, B.; Hourahine, B.; Frauenheim, T. DFTB+, a Sparse Matrix-Based Implementation of the DFTB Method. *J. Phys. Chem. A* **2007**, *111*, 5678−5684.
(51) Kresse, G.; Hafner, J. Ab Initio Molecular Dynamics for Liquid Metals. *Phys. Rev. B* **1993**, *47*, 558−561.
(52) Kresse, G.; Hafner, J. Ab Initio Molecular-Dynamics Simulation of the Liquid-Metal−Amorphous-Semiconductor Transition in Germanium. *Phys. Rev. B* **1994**, *49*, 14251−14269.
(53) Kresse, G.; Furthmüller, J. Efficiency of Ab-Initio Total Energy Calculations for Metals and Semiconductors Using a Plane-Wave Basis Set. *Comput. Mater. Sci.* **1996**, *6*, 15−50.
(54) Kresse, G.; Furthmüller, J. Efficient Iterative Schemes for Ab Initio Total-Energy Calculations Using a Plane-Wave Basis Set. *Phys. Rev. B* **1996**, *54*, 11169−11186.
(55) Blöchl, P. E. Projector Augmented-Wave Method. *Phys. Rev. B* **1994**, *50*, 17953−17979.
(56) Kresse, G.; Joubert, D. From Ultrasoft Pseudopotentials to the Projector Augmented-Wave Method. *Phys. Rev. B* **1999**, *59*, 1758−1775.
(57) Perdew, J. P.; Burke, K.; Ernzerhof, M. Generalized Gradient Approximation Made Simple. *Phys. Rev. Lett.* **1996**, *77*, 3865−3868.
(58) Perdew, J. P.; Burke, K.; Ernzerhof, M. Generalized Gradient Approximation Made Simple [Phys. Rev. Lett. 1996, 77, 3865]. *Phys. Rev. Lett.* **1997**, *78*, 1396−1396.
(59) Mermin, N. D. Thermal Properties of the Inhomogeneous Electron Gas. *Phys. Rev.* **1965**, *137*, A1441−A1443.
(60) Monkhorst, H. J.; Pack, J. D. Special Points for Brillouin-Zone Integrations. *Phys. Rev. B* **1976**, *13*, 5188−5192.
(61) Niklasson, A. M. N.; Tymczak, C. J.; Challacombe, M. Time-Reversible Born-Oppenheimer Molecular Dynamics. *Phys. Rev. Lett.* **2006**, *97*, 123001.
(62) Niklasson, A. M. N. Extended Born-Oppenheimer Molecular Dynamics. *Phys. Rev. Lett.* **2008**, *100*, 123004.
(63) Niklasson, A. M. N.; Steneteg, P.; Odell, A.; Bock, N.; Challacombe, M.; Tymczak, C. J.; Holmström, E.; Zheng, G.; Weber, V. Extended Lagrangian Born−Oppenheimer Molecular Dynamics with Dissipation. *J. Chem. Phys.* **2009**, *130*, 214109.
(64) Odell, A.; Delin, A.; Johansson, B.; Bock, N.; Challacombe, M.; Niklasson, A. M. N. Higher-Order Symplectic Integration in Born−Oppenheimer Molecular Dynamics. *J. Chem. Phys.* **2009**, *131*, 244106.
(65) Zheng, G.; Niklasson, A. M. N.; Karplus, M. Lagrangian Formulation with Dissipation of Born-Oppenheimer Molecular Dynamics Using the Density-Functional Tight-Binding Method. *J. Chem. Phys.* **2011**, *135*, 044122.
(66) Kirkpatrick, S.; Gelatt, C. D.; Vecchi, M. P. Optimization by Simulated Annealing. *Science* **1983**, *220*, 671−680.
(67) Černý, V. Thermodynamical Approach to the Traveling Salesman Problem: An Efficient Simulation Algorithm. *Journal of Optimization Theory and Applications* **1985**, *45*, 41−51.
(68) Caillabet, L.; Mazevet, S.; Loubeyre, P. Multiphase Equation of State of Hydrogen from *Ab Initio* Calculations in the Range 0.2 to 5 g/cm^3 up to 10 eV. *Phys. Rev. B* **2011**, *83*, 094101.
(69) Clay, R. C., III; McMinis, J.; McMahon, J. M.; Pierleoni, C.; Ceperley, D. M.; Morales, M. A. Benchmarking Exchange-Correlation Functionals for Hydrogen at High Pressures Using Quantum Monte Carlo. *Phys. Rev. B* **2014**, *89*, 184106.
(70) Loubeyre, P.; LeToullec, R.; Hausermann, D.; Hanfland, M.; Hemley, R. J.; Mao, H. K.; Finger, L. W. X-Ray Diffraction and Equation of State of Hydrogen at Megabar Pressures. *Nature* **1996**, *383*, 702−704.
(71) Nosé, S. A Unified Formulation of the Constant Temperature Molecular Dynamics Methods. *J. Chem. Phys.* **1984**, *81*, 511−519.
(72) Hoover, W. G. Canonical Dynamics: Equilibrium Phase-Space Distributions. *Phys. Rev. A* **1985**, *31*, 1695−1697.
(73) Sam, A.; Foulkes, W. M. C.; Thomas, D. K. Quantum Monte Carlo Study of High Pressure Solid Molecular Hydrogen. *New J. Phys.* **2013**, *15*, 113005.
(74) Becker, A.; Nettelmann, N.; Holst, B.; Redmer, R. Isentropic Compression of Hydrogen: Probing Conditions Deep in Planetary Interiors. *Phys. Rev. B* **2013**, *88*, 045122.
(75) Reed, E. J.; Fried, L. E.; Joannopoulos, J. D. A Method for Tractable Dynamical Studies of Single and Double Shock Compression. *Phys. Rev. Lett.* **2003**, *90*, 235503.
(76) Reed, E. J.; Fried, L. E.; Manaa, M. R.; Joannopoulos, J. D., A Multi-Scale Approach to Molecular Dynamics Simulations of Shock Waves. In *Chemistry at Extreme Conditions*; Manaa, M. R., Ed.; Elsevier: Amsterdam, 2005; pp 297−326.
(77) Reed, E. J.; Fried, L. E.; Henshaw, W. D.; Tarver, C. M. Analysis of Simulation Technique for Steady Shock Waves in Materials with Analytical Equations of State. *Phys. Rev. E* **2006**, *74*, 056706.
(78) Reed, E. J. Electron-Ion Coupling in Shocked Energetic Materials. *J. Phys. Chem. C* **2012**, *116*, 2205−2211.
(79) Mundy, C. J.; Curioni, A.; Goldman, N.; Will Kuo, I.-F.; Reed, E. J.; Fried, L. E.; Ianuzzi, M. Ultrafast Transformation of Graphite to Diamond: An Ab Initio Study of Graphite under Shock Compression. *J. Chem. Phys.* **2008**, *128*, 184701.

(80) Goldman, N.; Reed, E. J.; Kuo, I.-F. W.; Fried, L. E.; Mundy, C. J.; Curioni, A. Ab Initio Simulation of the Equation of State and Kinetics of Shocked Water. *J. Chem. Phys.* **2009**, *130*, 124517.
(81) Goldman, N.; Reed, E. J.; Fried, L. E. Quantum Mechanical Corrections to Simulated Shock Hugoniot Temperatures. *J. Chem. Phys.* **2009**, *131*, 204103.
(82) Qi, T.; Reed, E. J. Simulations of Shocked Methane Including Self-Consistent Semiclassical Quantum Nuclear Effects. *J. Phys. Chem. A* **2012**, *116*, 10451−10459.